J Solid State Electrochem (2012) 16:1247–1254
DOI 10.1007/s10008-011-1514-5

ORIGINAL PAPER

Electrochemical performance of rare-earth doped $LiMn_2O_4$ spinel cathode materials for Li-ion rechargeable battery

Huaibing Sun · Yungui Chen · Chenghao Xu · Ding Zhu · Lihong Huang

Received: 16 June 2011 / Revised: 17 July 2011 / Accepted: 23 July 2011 / Published online: 17 August 2011

Abstract Spinel powders of $LiMn_{2-x}RE_xO_4$ (RE = La, Ce, Nd, Sm; $0 \le x \le 0.1$) have been synthesized by solid-phase reaction. The structure and electrochemical properties of these electrode materials were characterized by X-ray diffraction (XRD), cyclic voltammetry (CV), electrochemical impedance spectroscopy (EIS) and charge–discharge experiment. The part substitution of rare-earth element RE for Mn in $LiMn_2O_4$ decreases the lattice parameter, resulting in the improvement of structural stability, and decreases the charge transfer resistance during the electrochemical process of $LiMn_2O_4$. As a result, the cycle ability, 55 °C high-temperature and high-rate performances of $LiMn_{2-x}RE_xO_4$ electrode materials are significantly improved with increasing RE addition, compared to the pristine $LiMn_2O_4$.

Keywords Li-ion battery · $LiMn_2O_4$ · Rare-earth · Doping

Introduction

By virtue of its higher energy density and free memory effect, lithium-ion battery (LIB) had become the best choice for electric vehicles (EV) and plug-in hybrid electric vehicles (PHEV) [1–3]. $LiMn_2O_4$ cathode material attracted great attention because it has rich and cheap starting materials, and because it is safe to use, environmentally friendly and has good rate capacity. But in the process of charging and discharging, the capacity of pure lithium manganese oxide will decay due to several factors such as Jahn–Teller distortion occurring on the surface of the particles and manganese dissolution into the electrolyte, especially at elevated temperatures. To overcome these drawbacks, two strategies were mainly pursued: elements substitution or oxygen excess to increase the oxidation state of Mn for suppressing the Jahn–Teller effect and surface modification or coating for suppressing the dissolution of manganese into the electrolyte [4–16]. The substitutions of rare earth elements for partial Mn in $LiMn_2O_4$ are attracting the attention of some researchers. Numerous studies have been conducted on heavy rare earth (Er, Sc, Y, etc.) doped $LiMn_2O_4$ [17–19]. Because heavy rare earth is expensive, light rare earth has drawn more attention recently. Arumugam and Kalaignan [20] studied the cycling performance of La-doped lithium manganese materials using the sol–gel method, and found that $LiLa_{0.05}Mn_{1.95}O_4$ has the best electrochemical performance. It delivers an initial discharge capacity of 125 mA hg^{-1} at 0.5C and a capacity retention of 89.6% after 50 cycles. Nd doped $LiMn_2O_4$ by chemical precipitation and calcination was researched by Singhal and Das [21], who reported that $LiNd_{0.01}Mn_{1.99}O_4$ has the highest discharge capacity (149 mA hg^{-1}) and has a capacity retention of about 91% after 25 cycles. Balaji and Mutharasu [22] synthesized $LiSm_xMn_{2-x}O_4$ by co-precipitation and microwave calcination. The cycle life study reveals a 93% capacity retention of $LiSm_{0.5}Mn_{1.95}O_4$ samples in comparison with 78.4% of $LiMn_2O_4$. To further clarify the influence of different light rare earth elements on the electrochemical properties of $LiMn_2O_4$, $LiMn_{2-x}RE_xO_4$ (RE = La, Ce, Nd, Sm; $0 \le x \le 0.1$), cathode materials were synthesized by conventional solid-phase methods, and their electrochemical performance was investigated in this study.

H. Sun · Y. Chen (✉) · C. Xu · D. Zhu · L. Huang
College of Materials Science and Engineering,
Sichuan University,
Chengdu 610065, China
e-mail: ygchen60@yahoo.com.cn

Experimental

$LiMn_2O_4$ sample was synthesized by solid-state reaction. A stoichiometric mixture of lithium carbonate (Li_2CO_3) and electrolytic manganese dioxide (EMD) was thoroughly mixed by high energy ball mill and calcined at 450 °C for 5 h, and then sintered at 750 °C for 13 h in air, followed by slow cooling to ambient temperature. $LiMn_{2-x}RE_xO_4$ (RE = La, Ce, Nd, Sm; $0 \le x \le 0.1$) samples were prepared using the same route with a starting molar ratio of Li/RE/Mn=1:x:2−x, where RE oxides were adopted.

The crystal structure and lattice parameter of the powders were determined by X-ray diffraction (XRD) using Cu Kα radiation in the range of 2θ=15–80° and the step size was 0.04°. To measure the electrochemical properties of $LiMn_2O_4$ and $LiMn_{2-x}RE_xO_4$ (RE = La, Ce, Nd, Sm; $0 \le x \le 0.1$), we used electrochemical cells that consisted of a $LiMn_{2-x}RE_xO_4$ as positive electrode, Li metal as the negative electrode, electrolyte of 1 M $LiPF_6$ in a 1:1(volume ratio) mixture of ethylene carbonate (EC) and dim ethyl carbonate (DMC), and Celgard 2400 membrane as the separator between cathode and anode. The cathode was a mixture of 85 wt.% $LiMn_{2-x}RE_xO_4$ active material, 8 wt.% acetylene black and 7 wt.% polyvinylidene fluoride (PVDF) dissolved in 1-methyl-2-pyrolidinone (NMP), which was spread on 14-mm-diameter aluminium foil and heated to 120 °C for 12 h in vacuum. The cells were assembled in argon-filled glove box. The CC–CV cycling was performed between 3.0 and 4.3 V with 0.5C rate on the Land CT2001A made in China. The cyclic voltammetric (CV) experiments between 3.2 and 4.5 V and electrochemical impedance spectroscopy (EIS) were carried out on Parstat 2273 (USA). After the cells were at the half-discharge state, the impedance spectra were recorded potentiostatically by applying an AC voltage of 5 mV amplitude over the frequency range 10^5 to 0.05 Hz.

Results and discussion

The powder XRD patterns of $LiMn_{2-x}RE_xO_4$ (RE = La, Ce, Nd, Sm; $0 \le x \le 0.1$) are shown in Fig. 1. The diffraction pattern of $LiMn_2O_4$ is in good agreement with that obtained from JCPDS file No.35-0782, which corresponds to the cubic spinel structure of *Fd3m* space group with the cell parameter of 8.248(4) Å. All doped samples possess the same cubic spinel structure in which Li^+ ions occupy the 8a tetrahedral sites, $Mn^{3+/4+}/RE^{3+/4+}$ ions occupy the 16d octahedral sites, and the O^{2-} ions occupy the 32e sites [23]. With the RE addition of x=0.1, the second phase of RE oxide appears, i.e., La_2O_3 for $LiMn_{1.9}La_{0.1}O_4$, CeO_2 for $LiMn_{1.9}Ce_{0.1}O_4$, Nd_2O_3 for $LiMn_{1.9}Nd_{0.1}O_4$ and Sm_2O_3 for

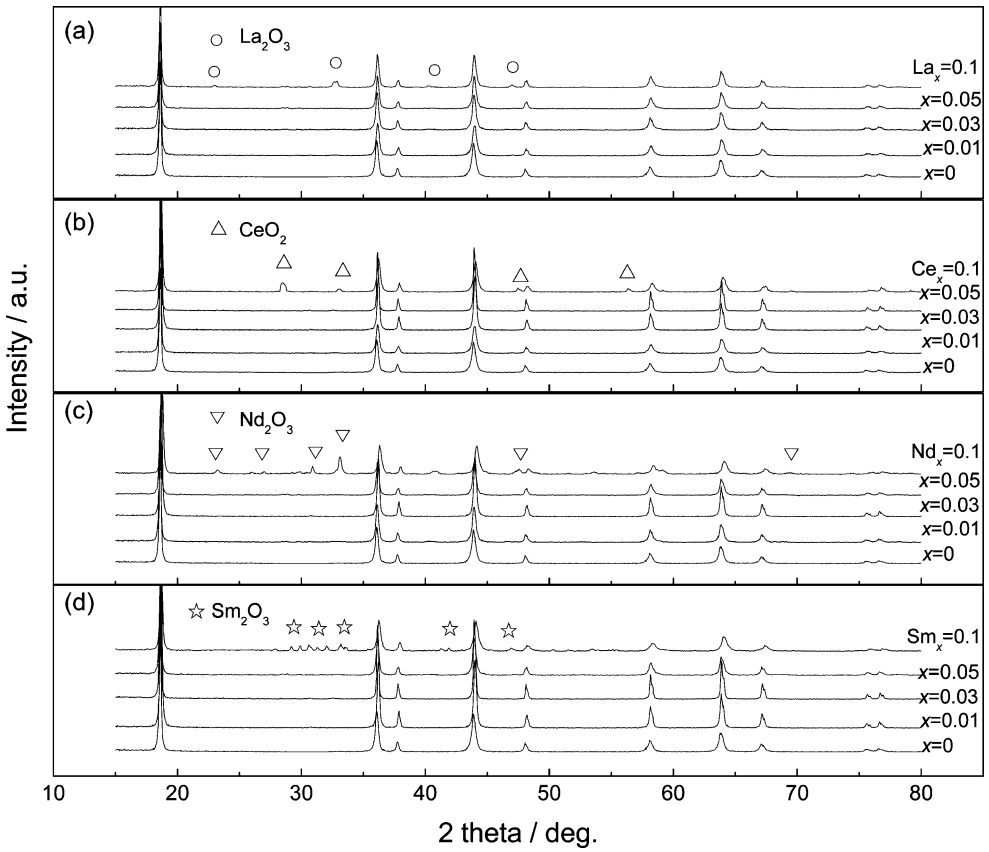

Fig. 1 Powder XRD patterns of $LiMn_{2-x}RE_xO_4$ (RE = La (**a**), Ce (**b**), Nd (**c**) or Sm (**d**); $0 \le x \le 0.1$)

Table 1 Cell parameters of $LiMn_{2-x}RE_xO_4$ (RE = La, Ce, Nd, Sm; $0 \le x \le 0.1$)

RE	a (Å)					V (Å^3)				
	x=0	x=0.01	x=0.03	x=0.05	x=0.1	x=0	x=0.01	x=0.03	x=0.05	x=0.1
La	8.247(1)	8.245(2)	8.243(1)	8.239(2)	8.224(7)	560.923(6)	560.536(0)	560.107(9)	559.313(3)	556.365(5)
Ce		8.243(4)	8.238(2)	8.231(4)	8.224(4)		560.169(1)	559.109(7)	557.726(3)	556.304(6)
Nd		8.241(7)	8.234(4)	8.225(5)	8.218(5)		559.822(6)	558.336(3)	556.527(9)	555.108(2)
Sm		8.241(5)	8.230(3)	8.223(7)	8.217(2)		559.781(8)	557.502(7)	556.162(6)	554.844(9)

$LiMn_{1.9}Sm_{0.1}O_4$. Their chemical rate were obtained from the Rietveld crystal structure program, and the impurities concentration are 2.3 wt.%, 1.8 wt.%, 2.5 wt.%, 2.7 wt.% for La_2O_3, CeO_2, Nd_2O_3 and Sm_2O_3, respectively.

The lattice parameters of $LiMn_{2-x}RE_xO_4$ are given in Table 1. It can be seen from Table 1 that the cell constant decreases with the increase in RE doping content. This effect may have resulted from the following factors. Although the ionic radii of RE is larger than that of Mn-ionic, which will lead to a slight increase of the lattice parameter, the bond energies of RE–O, namely, La^{3+}–O^{2-} (799 kJ mol^{-1}), Ce^{4+}–O^{2-} (795 kJ mol^{-1}), Nd^{3+}–O^{2-} (703 kJ mol^{-1}) and Sm^{3+}–O^{2-} (619 kJ mol^{-1}), are much stronger than that of Mn^{3+}–O^{2-}, which is only 402 kJ mol^{-1} [24], leading to the decrease of the lattice parameter. Similar results were also observed in La-doping [25], Ce-doping [26], Nd-doping [27] and Sm-doping [22] $LiMn_2O_4$.

Figure 2 shows the first charge–discharge curves and cycle performance of $LiMn_{2-x}RE_xO_4$ measured at 0.5C rate, and the results are summarized in Table 2. The two distinctive charge–discharge plateaus have been observed for all samples as shown in the inset of Fig. 2. The similar charge–discharge curves imply that rare earth-doped material does not change the electrochemical reaction

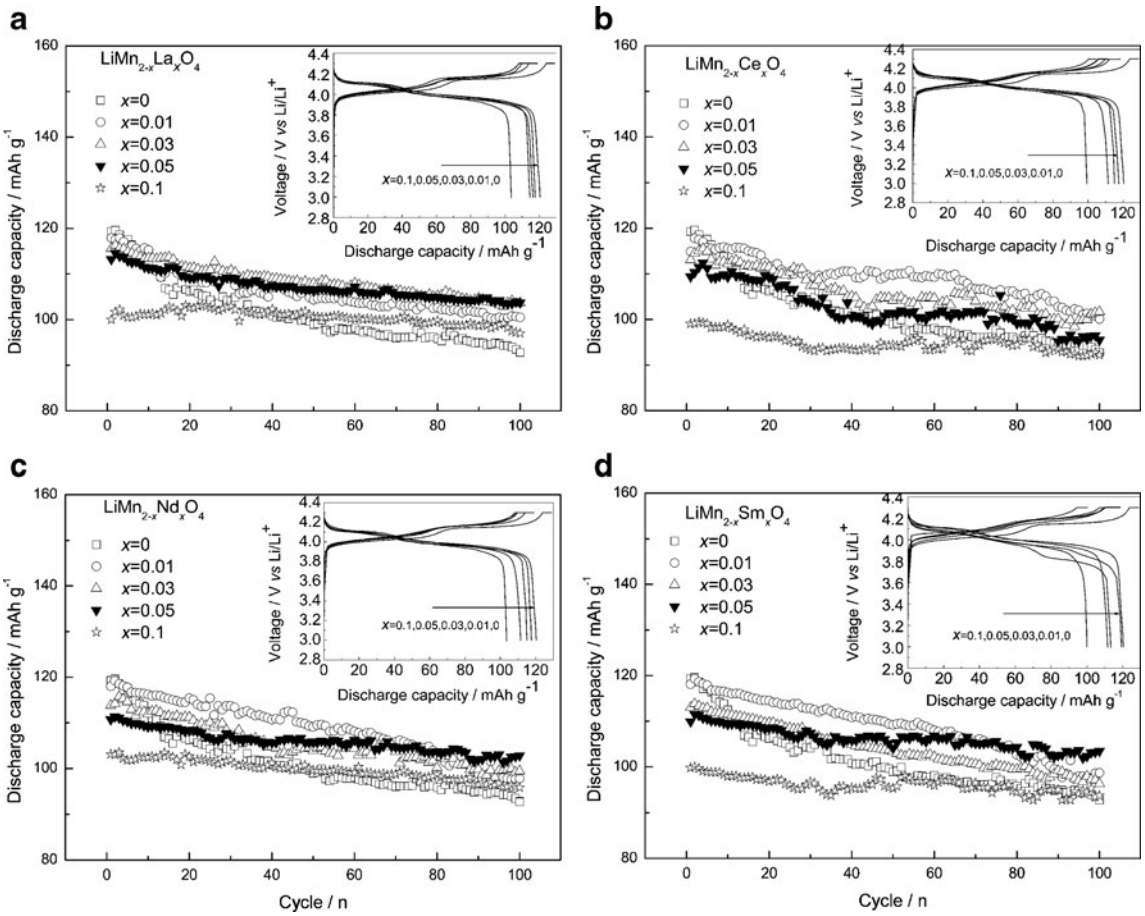

Fig. 2 The first charge–discharge and cycle curves of $LiMn_{2-x}RE_xO_4$ (RE = La (**a**), Ce (**b**), Nd (**c**) or Sm (**d**); $0 \le x \le 0.1$)

Table 2 Electrochemical performance of $LiMn_{2-x}RE_xO_4$ (RE = La, Ce, Nd, Sm; $0 \le x \le 0.1$)

Materials		RT				55 °C	
		C_0 (mA hg^{-1})	S_{100} (%)	HRD_{2C} (%)	HRD_{5C} (%)	C_0 (mA hg^{-1})	S_{50} (%)
$LiMn_2O_4$		119.3	77.8	78.5	45.4	127.4	75.3
$LiMn_{2-x}La_xO_4$	x=0.01	117.9	85.2	70.1	60.8	125.7	79.9
	x=0.03	115.6	89.7	86.1	69.6	119.7	82.1
	x=0.05	113.2	91.6	89.4	76.1	117.0	84.1
	x=0.10	100.0	96.9	88.3	73.7	101.4	94.5
$LiMn_{2-x}Ce_xO_4$	x=0.01	117.8	84.9	73.3	62.9	118.2	83.2
	x=0.03	114.5	88.8	82.9	70.3	115.8	85.9
	x=0.05	109.4	88.9	90.4	77.0	105.1	86.5
	x=0.10	99.1	93.2	91.8	57.3	101.2	92.3
$LiMn_{2-x}Nd_xO_4$	x=0.01	118.1	82.8	77.1	60.7	124.7	79.8
	x=0.03	114.0	87.3	86.1	69.7	115.0	86.1
	x=0.05	110.1	92.8	90.2	76.7	109.3	89.7
	x=0.10	99.4	95.8	88.3	73.2	101.3	91.2
$LiMn_{2-x}Sm_xO_4$	x=0.01	117.9	83.5	86.5	60.2	124.4	83.7
	x=0.03	113.0	85.2	88.3	62.7	119.3	86.6
	x=0.05	109.9	92.0	84.5	74.6	112.4	88.7
	x=0.10	99.8	93.8	86.4	73.6	102.1	92.2

RT room temperature, C_0 initial discharge capacity, S_{100} capacity retention after 100 cycles, S_{50} capacity retention after 50 cycles, HRD_{2C} high-rate dischargeability at the ratio of 2C discharge capacity vs. 0.2C discharge capacity, HRD_{5C} high-rate dischargeability at the ratio of 5C discharge capacity vs. 0.2C discharge capacity

mechanism of $LiMn_2O_4$. Different RE elements have a similar influence on the discharge and cycle stability of $LiMn_2O_4$. It can be seen in Table 2 that the initial discharge capacity of $LiMn_2O_4$ is about 120 mA hg^{-1}, which decreases slowly and linearly with x in $LiMn_{2-x}RE_xO_4$, increasing from 0.01 to 0.1, 118 mA hg^{-1} for x=0.01, 114 mA hg^{-1} for x=0.03, 110 mA hg^{-1} for x=0.05 and 100 mA hg^{-1} for x=0.1 on average. This influencing law can be expressed by Eq. 1, in which x represents x in $LiMn_{2-x}RE_xO_4$.

$$C_{o/0.5\,C} = 120 - 200x \quad (1)$$

However, it is clear from Fig. 2 that the cycle performance of $LiMn_2O_4$ electrode materials has an obvious improvement with the increasing concentration of RE. After 100 cycles, the capacity retention of $LiMn_2O_4$ is only 77.8%, while the capacity retention is 85.2% for $LiLa_{0.01}Mn_{1.99}O_4$, 89.7% for $LiLa_{0.03}Mn_{1.97}O_4$, 91.6% for $LiLa_{0.05}Mn_{1.95}O_4$ and 96.9% for $LiLa_{0.1}Mn_{1.90}O_4$. Similar results have also been found in Ce-, Nd- or Sm-doped $LiMn_2O_4$ materials, and their highest capacity retentions are 93.2% for $LiCe_{0.1}Mn_{1.90}O_4$, 95.8% for $LiNd_{0.1}Mn_{1.90}O_4$ and 93.8% for $LiSm_{0.1}Mn_{1.90}O_4$, respectively. The bonding energy between $RE^{3+/4+}$ and O^{2-} is higher than that of Mn^{3+}–O^{2-}, which improves the structural stability and enhances the cycle stability.

CV curves for the first cycle and 100th cycle at room temperature of $LiMn_{2-x}RE_xO_4$ are shown in Fig. 3. The curves of all samples are very similar, where the two pairs of the redox peaks coincide with the charge–discharge curves, presenting a typical electrochemical characteristic attributed to the two-step reversible intercalation and deintercalation processes of lithium ions in the 8a tetrahedral sites of spinel $LiMn_2O_4$ [28]. In the spinel $LiMn_2O_4$, the oxygen ions form a cubic closely packed array, and tetrahedral sites (8a) share a face with vacant octahedral sites (16c), so that they form three-dimensional vacant channels that allow Li ions to intercalate and deintercalate during the cathodic and anodic processes. In the oxidation process, the first peak is ascribed to the removal of Li ions from half of the tetrahedral sites in which Li–Li interactions exist, whereas the second peak is attributed to the removal of Li ions from the residual tetrahedral sites where Li ions do not have Li–Li interactions [29]. In the first cycle, two redox peaks were well separated as shown in Fig. 3a, and after the 100th cycle both anodic and cathode peaks were very close to each other with smaller intensity of peaks current compared to the first cycle, which is ascribed to possible Jahn–Teller distortion. It also can be found in Fig. 3a–f that the peak currents of the spinel oxide without doping decrease more quickly than those of the spinel oxides with RE doping after 100 cycles. It is apparent that

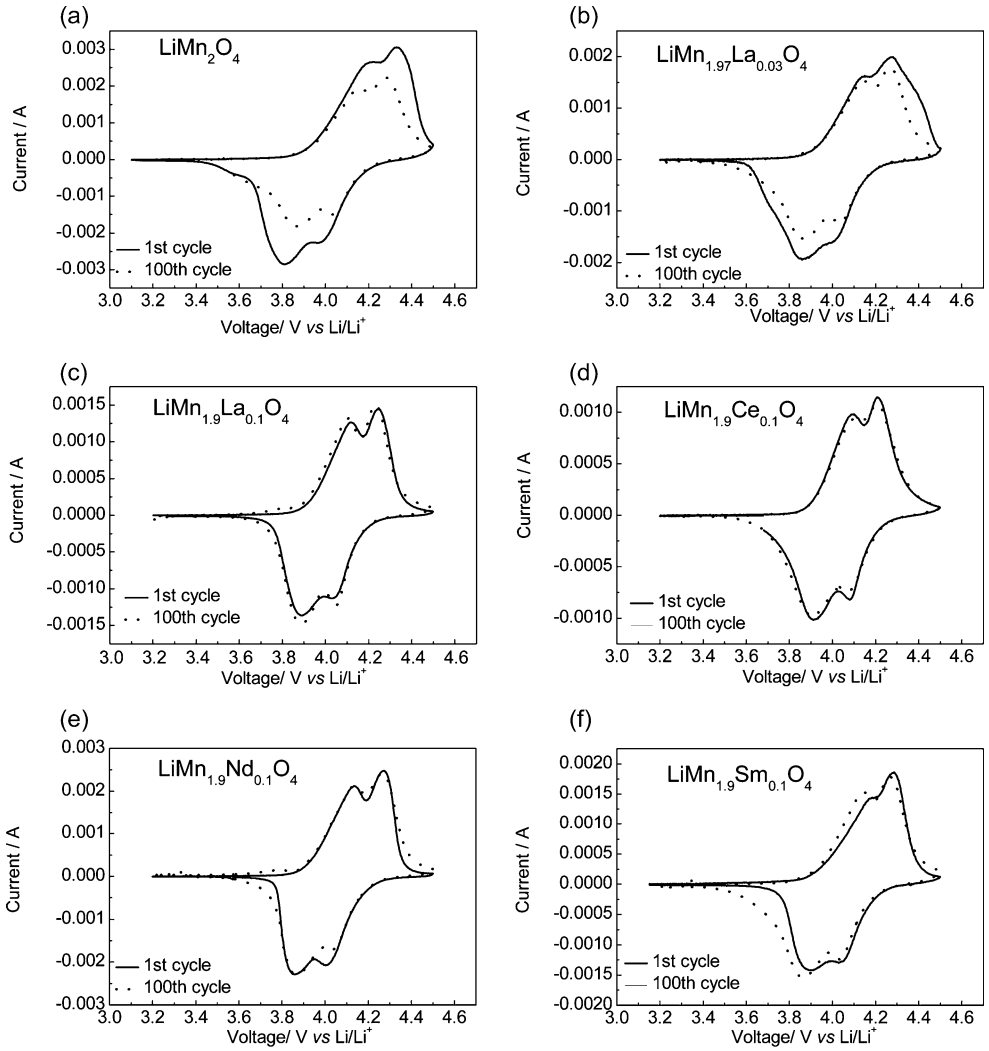

Fig. 3 Cyclic voltammograms of (**a**) $LiMn_2O_4$, (**b**) $LiMn_{1.97}La_{0.03}O_4$, (**c**) $LiMn_{1.9}La_{0.1}O_4$, (**d**) $LiMn_{1.9}Ce_{0.1}O_4$, (**e**) $LiMn_{1.9}Nd_{0.1}O_4$ and (**f**) $LiMn_{1.9}Sm_{0.1}O_4$ scanned at a rate of 0.02 mV/s

the cyclic stability of spinel lithium manganese oxide can be improved by doping of RE, which is a result of the improvement in structural stability and electrochemical performances. But compared to those without doping (Fig. 3a), high doping (Fig. 3b–f) will result in low intensity peaks current which leads to the decrease in area covered between oxidation and reduction peaks. Since the area is considered as the electrochemical active surface area, high doping will result in the reduction of initial discharge capacity, which is in accordance with the result shown in Fig. 2.

Figure 4 shows the comparison of the discharge capacities between undoping electrodes materials and electrodes materials with different contents of various RE at 55 °C. It can be seen in Fig. 4 that the lithium battery with doped electrode as the cathode active material has better rechargeability and cycleability than $LiMn_2O_4$ electrode, and all electrodes exhibited higher initial discharge capacity at 55 °C than that at room temperature. It can be seen from Fig. 4a that after cycling 50 times, the capacity retention is 75% for $LiMn_2O_4$, 79.9% for $LiMn_{1.99}La_{0.01}O_4$, 82.11% for $LiMn_{1.97}La_{0.03}O_4$, 84.1% for $LiMn_{1.95}La_{0.05}O_4$ and 94.5% for $LiMn_{1.90}La_{0.1}O_4$. Similar results can be observed in $LiMn_{2-x}RE_xO_4$ (RE = Ce, Sm, Nd) from Fig. 4b,c,d.

From the above analysis, it can be concluded that doping can obviously improve the electrochemical performance of the spinel-structure $LiMn_2O_4$. The result can be attributed to the following two factors. On one hand, rare earth doping decreases the lattice parameter, resulting in a more stable structure and the improvement of cycling performance. On the other hand, rare earth doping plays an important role in inhibiting the Jahn–Teller effect. Firstly, the rare earth ions have no Jahn–Teller effect. Moreover, the addition of rare earth ions changes manganese valence, leading to the redistribution of electron and a more symmetrical electron cloud on the d layer. The Jahn–Teller effect is thus effectively inhibited.

Figure 5 presents the discharge capacity of (a) $LiMn_{2-x}La_xO_4$, (b) $LiMn_{2-x}Ce_xO_4$, (c) $LiMn_{2-x}Nd_xO_4$ and (d) $LiMn_{2-x}Sm_xO_4$ at different rates. It can be seen from Fig. 5 that the pristine $LiMn_2O_4$ can retain more than 85% of its initial discharge capacity at the discharge

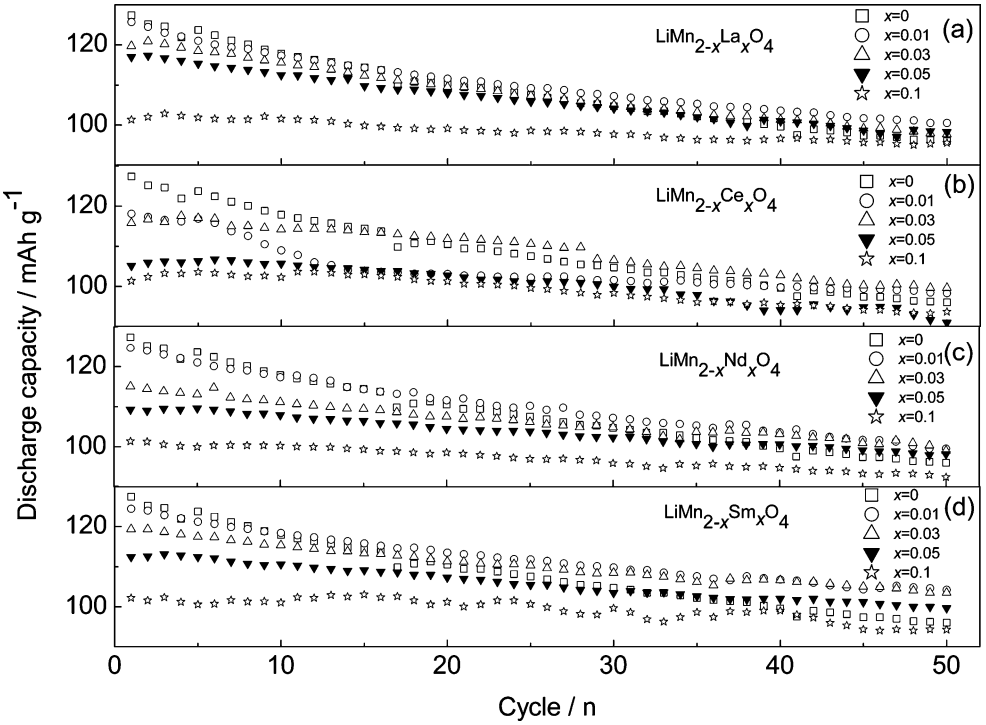

Fig. 4 Cycling performance of $LiMn_{2-x}RE_xO_4$ (RE = La (**a**), Ce (**b**), Nd (**c**) or Sm (**d**); $0 \le x \le 0.1$) at 55 °C

rate of 1C, but only 45% of its initial capacity could be delivered when discharge occurs at 5C. It is interesting to note that the rate performance of electrode materials has an obvious improvement with the increasing concentration of RE in all panels of Fig. 5 (a, b, c, d, $0 \le x \le 0.05$), and they can retain over 91% of their initial

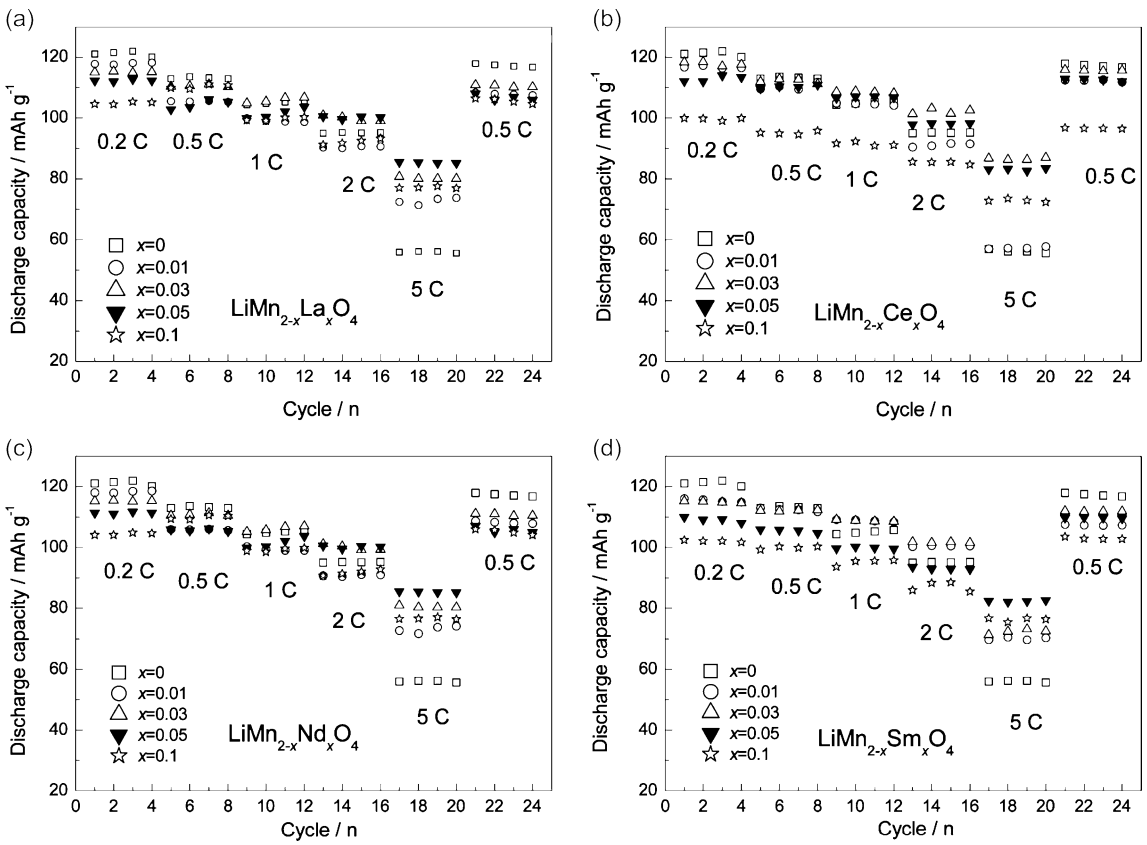

Fig. 5 Rate capacity of $LiMn_{2-x}RE_xO_4$ (RE = La (**a**), Ce (**b**), Nd (**c**) or Sm (**d**); $0 \le x \le 0.1$)

discharge capacity from 0.2 to 1C when x=0.05. At high discharge rate of 5C, $LiMn_{1.95}La_{0.05}O_4$, $LiMn_{1.95}Ce_{0.05}O_4$, $LiMn_{1.95}Nd_{0.05}O_4$ and $LiMn_{1.95}Sm_{0.05}O_4$ can still respectively retain 77%, 76%, 75% and 77% of their 0.2C initial discharge capacity, which are much higher than that of $LiMn_2O_4$. Discharge ability slightly decreased at 5C discharge rate with the doped concentration increasing to 0.1 compared to that when x=0.05. This may be ascribed to the second phase. The doping of RE may be the reason for excellent high rate performance of $LiMn_{1.95}RE_{0.05}O_4$ (RE = La, Ce, Nd, Sm), because of better electronic conductivity.

To further understand the improvement of the high rate discharge capability of the materials, electrochemical impedance spectra (EIS) were carried out in the half-discharged state after two cycles. The Nyquist plots of $LiMn_2O_4$ and $LiMn_{1.95}RE_{0.05}O_4$ are presented in Fig. 6. It can be seen that all plots consist of both a semicircle in the high middle frequency and a straight sloping line in the low frequency. The semicircle at high frequency is corresponding to a charge transfer step (R_{ct}), which may be ascribed to the charge transfer of lithium ion on the surface of spinel oxide because there are no other electrode reactions taking place during lithium insertion and removal in the oxide, and the electrode reaction process is mainly controlled by charge-transfer process [30]. The straight line at the low frequency is Warburg impedance (W_o), which is caused by the solid-phase diffusion in the electrode materials. The electrochemical parameters for all samples were obtained from equivalent circuit (Fig. 7) fitting of experimental data. In the equivalent circuit, R_s represents the solution resistance, C_{dl} is the double layer capacitance, R_{ct} is the resistance of charge transfer and W_o is Warburg impendence. The charge-transfer resistance (R_{ct}) in Fig. 6 decreases with the RE doping, 97 Ω for $LiMn_2O_4$, but 52, 67, 62 and 58 Ω for $LiMn_{1.95}La_{0.05}O_4$, $LiMn_{1.95}Ce_{0.05}O_4$, $LiMn_{1.95}Nd_{0.05}O_4$ and $LiMn_{1.95}Sm_{0.05}O_4$, respectively, which indicates that RE-doping could reduce the charge transfer resistance during the electrochemical process and improve high rate capability.

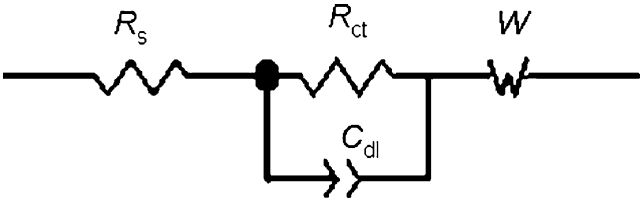

Fig. 7 The equivalent circuit diagram describing the kinetic process of lithium in spinel lithium manganese oxide

Conclusions

$LiMn_2O_4$ and $LiMn_{2-x}RE_xO_4$ (RE = La, Ce, Nd, Sm; $0 \le x \le 0.1$) are synthesized by solid-state reaction. XRD results showed that partial substitution of RE^{3+} for Mn in $LiMn_2O_4$ decreased the lattice parameter and improved the structural stability of $LiMn_2O_4$. Cyclic voltammograms and EIS analyses indicated that the charge–discharge polarization and charge transfer resistance were reduced after RE-doping, indicating enhanced kinetics performance of $LiMn_2O_4$ electrode. The cycle ability, high-temperature and high-rate performances of RE-doped $LiMn_2O_4$ electrode were significantly improved with increasing addition of RE^{3+}. The capacity retention of $LiMn_{1.9}RE_{0.1}O_4$ (RE = La, Ce, Nd, Sm, respectively) is 97%, 93%, 95% and 94% after 100th cycle at room temperature and 95%, 93%, 91%

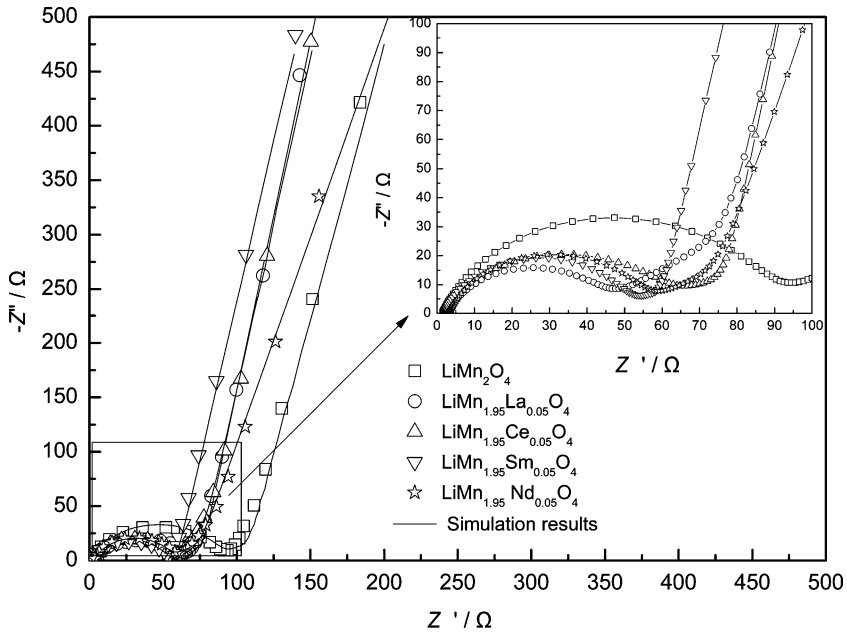

Fig. 6 Electrochemical impedance spectra (EIS) of $LiMn_2O_4$ and $LiMn_{1.95}RE_{0.05}O_4$ (RE = La, Ce, Nd or Sm)

and 92% after the 50th cycle at 55 °C. At a rate of 5C, 77%, 76%, 75% and 77% of the discharge capacity at 0.2C was maintained for $LiMn_{1.95}RE_{0.05}O_4$ (RE = La, Ce, Nd, Sm, respectively), which are much higher than the 45% rate for $LiMn_2O_4$. In a word, $LiMn_2O_4$ doping with RE showed excellent electrochemical performance as cathode material in Li-ion batteries.

References

1. Kitoh K (1999) J Power Sources 81–82:887–890
2. Horiba T, Matsumura J (2001) J Power Sources 97–98:719–721
3. Tatsumi K (2010) J Asian Electric Vehicles 8:1415–1418
4. Thackeray MM, Goodenough JB (1984) Mater Res Bull 19:179–187
5. Li XF, Xua YL, Wang CL (2009) J Alloys Compd 479:310–313
6. Zong HX, Cong CJ, Wang LN (2007) J Solid State Electrochem 11:195–200
7. Thackeray MM, Mansuetto MF, Dees DW (1996) Mater Res Bull 31:133–140
8. Sun YC, Wang ZX (2004) J Power Sources 132:161–165
9. Lee J (2000) H, Hong JK. J Power Sources 89:7–14
10. Ha HW, Yun NJ (2007) Electrochim Acta 52:3236–3241
11. Aurbach D, Levi MD, Gamulski K (1999) J Power Sources 81–82:472–479
12. Lee DJ, Lee KS (2011) J Power Sources 196:1353–1357
13. Amaral FA, Ricardo FB, Bocchi N (2010) J Power Sources 195:3293–3299
14. He XM, Li JJ (2005) J Solid State Electrochem 9:438–444
15. Yoshiaki M, Yosohiro S (2011) J Solid State Electrochem 15:503–510
16. Gnanaraj JS, Pol VG, Gedanken A (2003) Electrochem Commun 5:940–945
17. Liu HW, Zhang KL (2004) Mater Lett 58:3049–3051
18. Xie YT, Xu YB (2005) Solid State Ionics 176:2563–2569
19. Feng CQ, Tang H (2003) Mater Chem Phys 80:573–576
20. Arumugam D, Kalaignan GP (2008) Solid state Ionics 179:580–586
21. Singhal R, Das SR (2007) J Power Sources 164:857–861
22. Balaji SRK, Mutharasu D (2010) Ionics 16:351–360
23. Arora P, Popov BN, White RE (1998) J Electrochem Soc 145:807–815
24. Dean JA (ed) (1999) Lang's handbook of chemistry. McGraw-Hill, USA
25. Tu J, Zhao XB, Zhuang DG (2006) Physica B 382:129–134
26. Arumugam D, Kalaignan GP (2010) J Electroanal Chem 648:54–59
27. Hirose S, Kodera T, Ogihara T (2010) J Alloys Compd 506:883–887
28. Gao Y, Reimers JN, Dahn JR (1996) Phys Rev B 54:3878–3883
29. Xia YY, Yoshio M (1996) J Electrochem Soc 143:825–833
30. Ye SH, Bo JK, Li CZ (2010) Electrochim Acta 55:2972–2977